Optimally suppressed phonon tunneling in van der Waals graphene-WS_2 heterostructure with ultralow thermal conductivity

Wenyang Ding[1], Zhun-Yong Ong[2], Meng An[1], Brice Davier[1], Shiqian Hu[3], Masato Ohnishi[1], Junichiro Shiomi[1,4*]

[1] *Department of Mechanical Engineering, The University of Tokyo, 7-3-1 Hongo, Bunkyo, Tokyo 113-8656, Japan*

[2] *Institute of High Performance Computing, Agency for Science, Technology and Research (A*STAR), 1 Fusionopolis Way, #16-16 Connexis, Singapore 138632, Republic of Singapore*

[3] *School of Physics and Astronomy, Yunnan University, Kunming 650091, Peoples Republic of China*

[4] *Institute of Engineering Innovation, The University of Tokyo, 7-3-1 Hongo, Bunkyo, Tokyo 113-8656, Japan*

Email: shiomi@photon.t.u-tokyo.ac.jp

ABSTRACT: Van der Waals heterostructures have great potential for realizing ultimately low thermal conductivity because defect-less interfaces can be constructed at a length scale smaller than the phonon wavelength, allowing modulation of coherent phonon transport. In this letter, we demonstrate the mechanism for thermal conductivity reduction at a mode-resolved level. The graphene-WS_2 heterostructure with the lowest cross-plane thermal conductivity of 0.048 W/m-K is identified from 16384 candidate by combining Bayesian optimization and molecular dynamics simulations. Then, the angle-resolved phonon transmission is calculated using the mode-resolved atomistic Green's function. The results reveal that the optimal heterostructure nearly completely terminates phonon transport with finite incident angles owing to the reduced critical incident angle and suppression of phonon tunneling.

KEYWORDS: Van der Waals heterostructure, thermal transport, incident angle, phonon tunneling

The extraordinary properties of graphene, such as its high electrical conductivity, exceptional mechanical strength, optical transparency, make it highly promising for diverse applications [1,2]. Graphene's promising properties have encouraged researchers to explore the landscape of two-dimensional (2D) materials beyond graphene. Transition-metal dichalcogenide (TMDC) materials, whose chemical formula is MX_2 (M = Mo or W and X = S, Se, or Te), have also attracted tremendous attention owing to their excellent thermal and electrical properties [3]. With advances in synthesis technology, van der Waals (vdW) heterostructures can be fabricated by stacking 2D materials [4]. VdW heterostructures not only address graphene's zero-bandgap limitation but also serve as highly efficient thermal insulators [5] and thermal transistors [6].

Thermal properties optimization of materials is crucial for efficient energy conversion, enhanced thermal insulation, and the development of multifunctional materials for various technological advancements [7-9]. Phonons are the main quasiparticles that mediate thermal conduction in semiconductors and insulators. Therefore, phonon engineering, which refers to the manipulation and control of phonons to obtain targeted thermal properties, has attracted significant attention. Common phonon engineering strategies using impurities [10], nanoparticles [11,12], defects [13], and inclusions [14,15] are based on solving the Boltzmann transport equation, which treats phonons as particles. However, these phonons scatter effectively only across a confined frequency spectrum, typically in the high-frequency range [16]. A key approach to achieve broad spectrum impedance involves modifying coherent phonon waves using nanostructures, such as creation of phonon interference [17], forbidden phononic band gaps [18] and phonon localization [19].

The ability to lower thermal conductivity in superlattices by manipulating coherent phonon transport has been further demonstrated using material informatics [20,21]. Ju et al. [20] combined machine learning (ML) and the atomistic Green's function (AGF) to obtain an optimal Si/Ge heterostructure with minimum thermal conductance, which was attributed to the inhibition of constructive phonon interference. Assisted by ML, Hu et al. [21] experimentally determined an aperiodic GaAs/AlAs heterostructure with significantly lower thermal conductivity than their periodic counterparts. A major challenge in investigating phonon coherence in these heterostructures is the requirement for smooth interfaces with a roughness that is smaller than the phonon coherent length to avoid phonon phase breaking and phonon-phonon interactions.

The extremely smooth interfaces of vdW heterostructures present them as an ideal

platform for investigating coherent phonon. Strategies for engineering coherent phonon transport in vdW heterostructures include modification of the interlayer rotation [22-24], cross-plane strain [25], interlayer contact area [9], and stacking order [7,26]. For example, by combining Bayesian optimization with molecular dynamics simulations, a graphene/MoS_2 heterostructure with an ultralow thermal conductivity at room temperature was obtained owing to strong Anderson localization [7]. However, because the calculated phonon transmission was not mode (angle) resolved, the precise mechanism of the system was not understood.

This letter aims to develop a mechanism for lowering the cross-plane thermal conductivity of graphene-WS_2 vdW heterostructures. By combining Bayesian optimization and nonequilibrium molecular dynamics (NEMD) simulations, we identify the optimal stacking order for minimizing thermal conductivity. We adopt a graphene-WS_2 heterostructure owing to its large mass mismatch, and WS_2 is chosen based on its high Seebeck coefficient [27,28] and comparatively low thermal conductivity [29,30], making it a good candidate for thermoelectric applications. Among TMDC materials, WS_2 is expected to have the highest mobility due to the reduced effective mass [31] and low thermal conductivity due to high average atomic mass [32]. Using the mode-resolved AGF method, the heat conduction in the vdW heterostructures is resolved to the level of individual phonon polarizations, whose incident angles are utilized to elucidate the role of phonon tunneling.

Our approach contains three crucial components. First, each graphene/WS_2 heterostructure consists of a random arrangement of graphene and WS_2 layers. The unit cell parameters for graphene and WS_2 are set to 4.260 Å × 2.460 Å and 5.520 Å × 3.187 Å, respectively. To create the heterostructure supercell, we utilize a 13 × 22 unit cell configuration (55.39 Å × 54.12 Å) for graphene and a 10 × 17 unit cell configuration (55.20 Å × 54.18 Å) for WS_2. To eliminate the remaining mismatch in the supercell, a small strain within 1% (0.3% and 0.1% in the *x* and *y* direction, respectively) is introduced in graphene: the strain is sufficiently small as to not affect the cross-plane thermal conductivity [7,33], which is demonstrated in Fig. S1 and Fig. S2 of Supplemental Material. Subsequently, the LAMMPS package [34] is employed for the NEMD simulations (details in Supplemental Material).

To determine the heterostructure configuration with the lowest cross-plane thermal conductivity, we perform machine-learning-based structural optimization [7] which combines thermal conductivity calculations and Bayesian optimization [35]. A binary

array representation (descriptors) is utilized to describe each potential heterostructure; the graphene and WS_2 layers are labeled as "0" and "1", respectively. We fix the number of layers to $N = 14$ for a total number of potential candidates of 2^N or 16,384. By taking the 20 initial structures as the original training dataset and calculating their thermal conductivities using NEMD simulations, we employ Thompson sampling to predict the next 10 candidate structures from the candidate pool according to their probability of being optimal (details in Supplemental Material).

The optimized heterostructure is analyzed using the mode-resolved AGF method adopted in Ref. [36]. While the NEMD calculations have the advantage of naturally including all orders of anharmonicity in phonon-phonon scattering [37], the dynamics are treated classically and quantum effects are not considered. By contrast, the AGF approach, which considers quantum statistics, offers a straightforward means of tracking the behavior of phonons within a given frequency range. By utilizing the AGF approach, we can better understand the mechanism behind thermal conductivity reduction in terms of phonon behavior [38]. Therefore, the lattice thermal conductivity of pristine WS_2, pristine graphite, periodic superlattice, and optimized heterostructures are calculated using the mode-resolved AGF method. Because of the huge computational load required to calculate the force-constant matrix and the transmission function in heterostructures being of the same size as those considered in the NEMD study, we perform mode-resolved AGF calculations for a smaller heterostructure with a reduced cross-section. Within the mode-resolved AGF framework [39,40], the system is partitioned into three interconnected components: left and right semi-infinite leads and the central device region. The left and right leads consist of an infinite array of double-layer graphene or graphite, whereas the center region consists of a heterostructure. Details regarding the mode-resolved AGF are provided in the Supplemental Material and Ref. [36]. Then, the temperature-dependent thermal conductance per unit area $\sigma(T)$ for the device region is calculated in the Landauer formalism [41,42] (Supplemental Material).

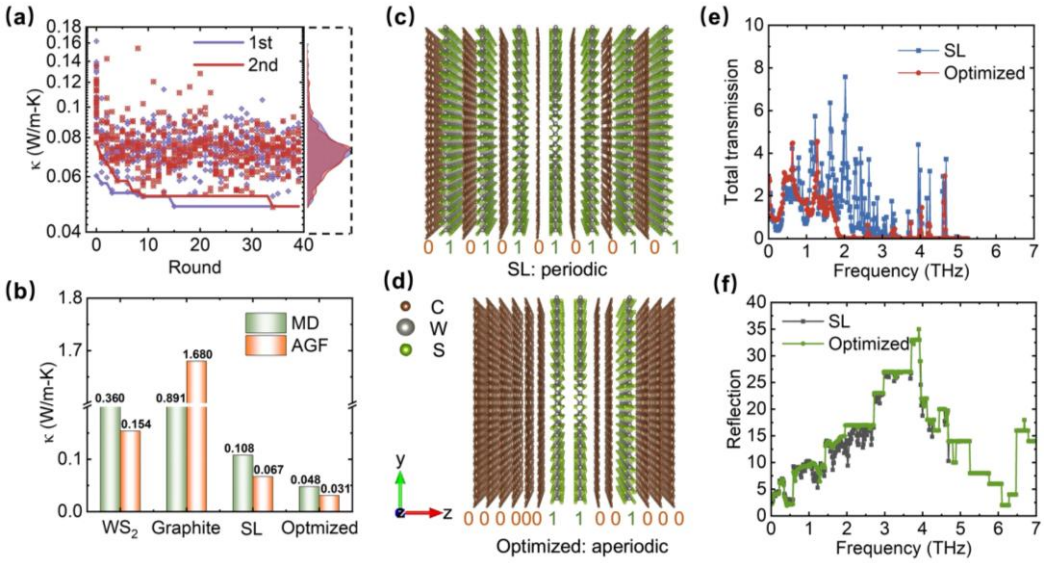

FIG. 1. (a) Variation of thermal conductivities during Bayesian optimization. (b) Thermal conductivities obtained by NEMD and mode-resolved AGF for graphene-WS_2 (periodic) superlattice and (a-periodic) optimized heterostructure. The structure of the (c) superlattice and (d) optimized heterostructure. The dependence of (e) transmission and (f) reflection on frequency for the superlattice and optimized heterostructures.

Figure 1(a) shows the optimization procedure combining Bayesian optimization of the stacking order and NEMD simulations for determining the graphene-WS_2 heterostructure with the lowest thermal conductivity, performed twice with different initial candidates to minimize the stochastic influence. The curves in the dashed box on the right show the thermal conductivity probability distributions for the two optimization procedures [20]. The results yield an optimized heterostructure with the lowest thermal conductivity of 0.048 W/(m·K), which is only 5% of graphite thermal conductivity (Fig. 1(b)). This value is of the same magnitude as the cross-plane thermal conductivity obtained by controlling stacking order in the previous studies [28][29]. In addition, the 95% reduction is substantial compared to the 50% reduction achieved through modifications in rotation angle [22], strain [25], and insertion [43], demonstrating that the controllability by heterostructure is larger. Interestingly, the thermal conductivity of the optimized heterostructure (00000011001000, shown in Fig. 1(d)) is only half that of the corresponding periodic superlattice (01010101010101, shown in Fig. 1(c)); however, the former has significantly fewer heterointerfaces. Since such graphene-WS_2 vdW heterostructures haven't fabricated experimentally, we evaluated the thermal stability of superlattice and optimized heterostructure, as shown in Fig. S3. Moreover, we have performed calculations of the thermal conductivity of materials consisting of many repetitions of the layer stack using NEMD simulations, as shown in Fig. S4,

which indicates the conclusion on the effectiveness of the optimization can be extended to larger sized system.

Figure 1(b) shows the thermal conductivity results obtained using mode-resolved AGF, which are similar to those obtained using NEMD. The reason behind the similar thermal conductivity values calculated by NEMD and AGF despite the difference in classical/quantum statistics is illustrated in Fig. S5.

The frequency-dependent transmission spectrum obtained using AGF is displayed in Fig. 1(e). We observe that, except for certain frequencies below 1 THz, the transmission spectrum of the optimized heterostructure is smaller over the full frequency range than that of the superlattice. The low frequency phonons (< 1 THz) do not account for the thermal conductivity difference between superlattice and optimized heterostructure, as shown in Fig. S6. This conclusion remains valid even as the system thickness increases, as demonstrated in Fig. S7. Figure 1(f) shows the calculated phonon reflection, which is essential for understanding the interface scattering of phonons. The phonon reflection of the optimized heterostructure is clearly higher than that of the superlattice, which explains the low phonon transmission in the optimized heterostructure. To understand the mechanism underlying the high reflection in the aperiodic-optimized heterostructure, the phonon transmission spectra of the periodic superlattice and aperiodic-optimized heterostructure are decomposed mode-wise.

It has been extensively documented that flexural phonons contribute remarkably to the in-plane thermal conductivity of 2D materials and that interfacial scattering is the main factor accounting for the reduced in-plane thermal conductivity of substrate-supported 2D materials [44-46]. By contrast, there has been much less investigation into the role of flexural phonons in out-of-plane thermal conductivity [47,48]. Therefore, we evaluate the thermal conductivity contributions of different phonon branches for the superlattice and optimized heterostructure. Due to the additional interlayer interactions, the out-of-plane acoustic modes in graphite deviate from the quadratic dispersion relation of ZA mode in graphene [49], resulting in quasi-flexural behavior [50]. These out-of-plane quasi-flexural modes in graphite are conventionally referred to as longitudinal acoustic (LA) phonons (detailed explanation in Supplemental Material) [51-54]. We use a two-stage hybrid algorithm [55] to distinguish the branches. Figure 2(a) and 2(b) show that the LA phonon contribution dominates in both heterostructures and accounts for the difference in thermal conductivity. Therefore, we focus on the transport of LA phonons. At the same time, since there is non-negligible contribution from LO'

phonons to thermal conductivity, the contribution of LO' phonons are discussed in Supplemental Material (Fig. S8).

Before proceeding with the analysis, we clarify two concepts [56,57]. The first concept is that of the critical angle (Fig. 2(c)). Phonons with incident angles larger than the critical angle undergo total reflection without refraction. However, an evanescent wave is nevertheless transmitted to the other side of the interface despite total reflection. As

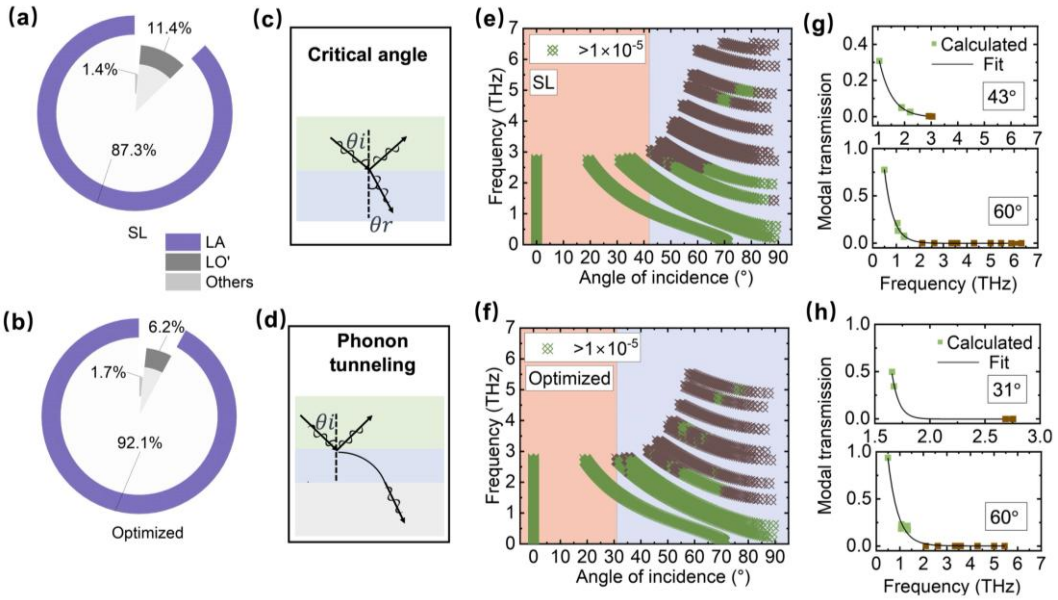

FIG. 2. Thermal conductivity contribution of different phonon branches for (a) superlattice and (b) optimized heterostructure. The schematic of (c) critical angle and (d) phonon tunneling. The dependence of LA phonon modal transmission on frequency and angle of incidence for (e) superlattice and (f) optimized heterostructure, respectively. (g) The dependence of phonon modal transmission on frequency for superlattice at 43° and 60°. (h) The dependence of phonon modal transmission on frequency for optimized heterostructure at 31° and 60°.

illustrated in Fig. 2(d), phonon tunneling occurs if the evanescent wave refracts into a third medium (the bottom gray part) before being completely damped and becoming a propagating mode, which causes the phonon transmission for the mode to no longer be zero. Previous studies discussed the effects of phonon tunneling on thermal transport in the context of long-range Coulombic forces [58,59]. For example, Igor et al. [58] invoked the interfacial electric field-induced phonon tunneling mechanism to explain interfacial thermal transport. This study investigates the effects of critical angle and phonon tunneling on thermal transport in vdW heterostructures for the first time.

Figure 2(e) shows the dependence of the LA phonon modal transmission in the superlattice on frequency and incident angle. Modal transmissions that fall below 1×10^{-5} (denoted by brown symbols) are regarded as total reflection with negligible

contribution to thermal transport. The extracted modal transmission values for the superlattice and optimized heterostructure are shown in Fig. S10. When the angle of incidence is larger than 43°, some phonon modes are totally reflected. Therefore, the critical angle for the LA phonons in the superlattice is 43°, and the nonzero modal transmission at larger angles of incidence is due to phonon tunneling. Similarly, as shown in Fig. 2(f), the critical angle for the LA phonons in the optimized heterostructure is 31°, which is smaller than that of the superlattice.

We confirm the presence of phonon tunneling through the frequency dependence of the modal transmission, displayed in Fig. 2(g) and 2(h) (the dependence of phonon modal transmission on frequency for the optimized heterostructure at 43° is shown in Fig. S11). The frequency shows an exponential decay, which is characteristic to phonon tunneling [56,57]. By contrast, the dependence of the phonon modal transmission on the frequency does not decay exponentially when the angle of incidence is lower than the critical angle (Fig. S12).

To visualize how the critical angle and phonon tunneling can be controlled by nanostructuring, we compare the modal transmissions of the superlattice and optimized heterostructure in detail by selecting two representative frequencies in the higher (2.42 THz) and lower (1.16 Hz) frequency regimes, which correspond to the cases with and without phonon tunneling. Figure 3 shows the wave vectors in the Brillouin zone of graphite and the corresponding transmission. For the superlattice, the higher-frequency case in Fig. 3(a) shows a clear contrast in the transmission between the interior and exterior of the critical cone, which confirms that only phonons with wave vectors within the critical angle can be transmitted. By contrast, in the case of the lower frequency shown in Fig. 3(b), the phonon modes outside the critical cone exhibits large transmission owing to phonon tunneling.

In the optimized heterostructure, the transmission is largely modulated by the arrangement of the graphene and WS_2 layers between the graphite leads. At the higher frequency shown in Fig. 3(c), phonons with wave vectors inside the critical cone are fully suppressed owing to the stopbands formed by destructive phonon interference (Fig. S12 (b) and (d)). The stop bands are analogous to optical stop bands and are associated with minigaps in the phonon spectra [56]. At a lower frequency, the transmission in the

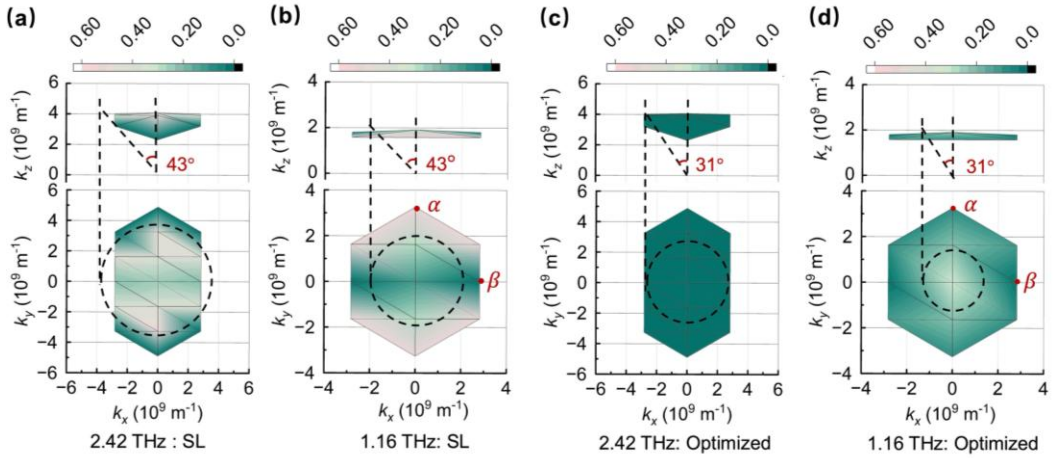

FIG. 3. Wave vectors in the Brillouin zone of graphite lead and their corresponding transmission. The dashed circle represents the top view of the critical cone obtained by rotation of the critical angle (denoted by the red arc), and the grid nodes represent wave vector points. Modal transmission for the superlattice at (a) 2.42 THz and (b) 1.16 THz. Modal transmission for the optimized heterostructure at (c) 2.42 THz and (d) 1.16 THz.

superlattice (Fig. 3(b)) due to phonon tunneling is substantially suppressed for wave vectors outside the critical cone in the optimized heterostructure (Fig. 3 (d)). For instance, the transmission of the phonon mode at α (64°) and β (57°) in Fig. 3(b) and (d) is suppressed from 0.503 to 0.089 and from 0.023 to 0.006, respectively. These findings clarify how the optimized heterostructure attenuates phonon tunneling.

These results reveal that the optimized heterostructure impedes phonon transport by enhancing destructive phonon interference, reducing the critical angle, and suppressing phonon tunneling. The impact of these characteristics on thermal conductivity can be evaluated by comparing the dependence of the phonon transmission on the angle of incidence for the superlattice and the optimized heterostructure, as shown in Fig. S13. The differences in thermal conductivity between the superlattice and the optimized heterostructure attributed to enhanced phonon interference (0–31°), reduced critical angle (31–43°), and suppressed phonon tunneling (43–90°) are 0.004 W/(m·K), 0.006 W/(m·K), and 0.024 W/(m·K), respectively. Therefore, we conclude that the low

transmission of the optimized heterostructure is mainly due to the suppression of phonon tunneling. Lastly, we simply provide the experimental feasibility of our research in the Supplemental Material.

Through Bayesian optimization of the stacking order and NEMD simulations, the aperiodic-optimized graphene-WS_2 heterostructure with an ultralow thermal conductivity of 0.048 W/(m·K) is identified from 16384 candidates. To elucidate the underlying mechanism, the mode-wise phonon transmission through the aperiodic-optimized heterostructure and periodic superlattice is directly examined using the mode-resolved AGF method. The results show that for both the optimized heterostructure and superlattice, LA phonons dominate the cross-plane heat transport. Analysis of the dependence of the phonon transmission on the incident angle and frequency shows that the ultralow thermal conductivity originates from the controllability of suppressing phonon tunneling. These findings yield physical insight into how broad-spectrum and angle-phonon transports can be terminated.

Supporting Information: Details of NEMD simulations, machine-learning-based optimization, and mode-resolved AGF calculation; influence of strain on thermal conductivity; thermal stability; size dependence; influence of classical/quantum distribution; modal contribution to thermal conductivity; phonon dispersion of lead and graphene-WS_2 vdW heterostructures; modal transmission and its dependence on frequency and incident angle; temperature dependence; discussion of experimental feasibility.

ACKNOWLEDGMENTS

This work was partially supported by KAKENHI (Grant No. 22KJ0627) from the Japan Society for the Promotion of Science (JSPS) and CREST (Grant no. JPMJCR21O2), provided by the Japan Science and Technology Agency (JST). W. D. acknowledges the support from the JSPS Research Fellowship for Young Scientists (Grant No. 21J21382). Z.-Y. O. acknowledges funding support from the Agency for Science, Technology and Research (A*STAR) of Singapore with the Manufacturing, Trade and Connectivity (MTC) Programmatic Grant “Advanced Modeling Models for Additive Manufacturing” (M22L2b0111) and from the Polymer Matrix Composites Program (SERC Grant No. A19C9a004). Numerical calculations were performed at the facilities of the Supercomputer Center, Institute for Solid-State Physics, University of Tokyo, and

MASAMUNE-IMR at the Center for Computational Materials Science, Institute for Materials Research, Tohoku University (Project No. 2112SC0507).

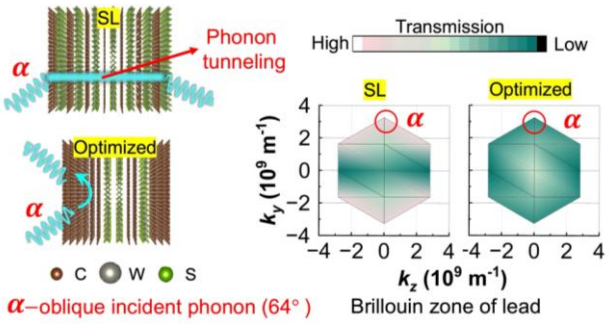

TOC Graphic

REFERENCES

1 Wu, Z.-S. *et al.* Synthesis of Graphene Sheets with High Electrical Conductivity and Good Thermal Stability by Hydrogen Arc Discharge Exfoliation. *ACS Nano* **3**, 411-417 (2009). https://doi.org:10.1021/nn900020u

2 Li, X., Yu, J., Wageh, S., Al-Ghamdi, A. A. & Xie, J. Graphene in Photocatalysis: A Review. *Small* **12**, 6640-6696 (2016). https://doi.org:https://doi.org/10.1002/smll.201600382

3 Sorkin, V., Pan, H., Shi, H., Quek, S. Y. & Zhang, Y. W. Nanoscale Transition Metal Dichalcogenides: Structures, Properties, and Applications. *Crit. Rev. Solid State* **39**, 319-367 (2014). https://doi.org:10.1080/10408436.2013.863176

4 Geim, A. K. & Grigorieva, I. V. Van der Waals Heterostructures. *Nature* **499**, 419-425 (2013). https://doi.org:10.1038/nature12385

5 Vaziri, S. *et al.* Ultrahigh Thermal Isolation across Heterogeneously Layered Two-dimensional Materials. *Sci. Adv.* **5**, eaax1325 (2019). https://doi.org:10.1126/sciadv.aax1325

6 Sood, A. *et al.* An Electrochemical Thermal Transistor. *Nat. Commun.* **9**, 4510 (2018). https://doi.org:10.1038/s41467-018-06760-7

7 Hu, S. *et al.* Ultimate Impedance of Coherent Heat Conduction in Van der Waals Graphene-MoS_2 Heterostructures. *Mater. Today Phys.* **16**, 100324 (2021). https://doi.org:https://doi.org/10.1016/j.mtphys.2020.100324

8 Spiece, J. *et al.* Low Thermal Conductivity in Franckeite Heterostructures. *Nanoscale* **14**, 2593-2598 (2022). https://doi.org:10.1039/D1NR07889E

9 Jia, P.-Z. *et al.* Excellent Thermoelectric Performance Induced by Interface Effect in $MoS_2/MoSe_2$ Van der Waals Heterostructure. *J. Phys. Condens. Matter* **32**, 055302 (2019). https://doi.org:10.1088/1361-648X/ab4cab

10 Chen, S. *et al.* Thermal Conductivity of Isotopically Modified Graphene. *Nat. Mater.* **11**, 203-207 (2012).

11 Lin, Z. *et al.* Scalable Solution-phase Epitaxial Growth of Symmetry-mismatched Heterostructures on Two-dimensional Crystal Soft Template. *Sci. Adv.* **2**, e1600993 https://doi.org:10.1126/sciadv.1600993

12 Nutz, F. A. & Retsch, M. Tailor-made Temperature-dependent Thermal Conductivity via Interparticle Constriction. *Sci. Adv.* **3**, eaao5238 https://doi.org:10.1126/sciadv.aao5238

13 Hao, F., Fang, D. & Xu, Z. Mechanical and Thermal Transport Properties of Graphene with Defects. *Appl. Phys. Lett.* **99**, 041901 (2011). https://doi.org:10.1063/1.3615290

14 Qian, X., Gu, X., Dresselhaus, M. S. & Yang, R. Anisotropic Tuning of Graphite Thermal Conductivity by Lithium Intercalation. *J. Phys. Chem. Lett.* **7**, 4744-4750 (2016).

15 Koley, S., Sen, S. & Chakrabarti, S. Vanishing Thermal Conductance of Carbon Nanotube Upon Encapsulation by Zigzag Sulfur Chain. *J. Phys. Chem. Lett.* **9**, 3105-3109 (2018).

16 Xiong, S. *et al.* Blocking Phonon Transport by Structural Resonances in Alloy-Based Nanophononic Metamaterials Leads to Ultralow Thermal Conductivity. *Phys. Rev. Lett.* **117**, 025503 (2016). https://doi.org:10.1103/PhysRevLett.117.025503

17 Jiang, P. *et al.* Total-transmission and total-reflection of individual phonons in phononic crystal nanostructures. *APL Materials* **9** (2021). https://doi.org:10.1063/5.0046509

18 Hu, S. *et al.* Two-path phonon interference resonance induces a stop band in a silicon crystal matrix with a multilayer array of embedded nanoparticles. *Phys. Rev. B* **102**, 024301 (2020). https://doi.org:10.1103/PhysRevB.102.024301

19 Hu, S. *et al.* Disorder limits the coherent phonon transport in two-dimensional phononic crystal structures. *Nanoscale* **11**, 11839-11846 (2019). https://doi.org:10.1039/C9NR02548K

20 Ju, S. *et al.* Designing Nanostructures for Phonon Transport via Bayesian Optimization. *Phys. Rev. X* **7**, 021024 (2017). https://doi.org:10.1103/PhysRevX.7.021024

21 Hu, R. *et al.* Machine-Learning-Optimized Aperiodic Superlattice Minimizes Coherent Phonon Heat Conduction. *Phys. Rev. X* **10**, 021050 (2020). https://doi.org:10.1103/PhysRevX.10.021050

22 Ren, W. *et al.* The Impact of Interlayer Rotation on Thermal Transport Across Graphene/Hexagonal Boron Nitride van der Waals Heterostructure. *Nano Lett.* **21**, 2634-2641 (2021). https://doi.org:10.1021/acs.nanolett.1c00294

23 Kim, S. E. *et al.* Extremely Anisotropic Van der Waals Thermal Conductors. *Nature* **597**, 660-665 (2021). https://doi.org:10.1038/s41586-021-03867-8

24 Ren, W. *et al.* Impact of moiré superlattice on atomic stress and thermal transport in van der Waals heterostructures. *Applied Physics Reviews* **10** (2023). https://doi.org:10.1063/5.0159598

25 Wu, X. & Han, Q. Phonon Thermal Transport across Multilayer Graphene/Hexagonal Boron Nitride van der Waals Heterostructures. *ACS Appl. Mater. & Interfaces* **13**, 32564-32578 (2021). https://doi.org:10.1021/acsami.1c08275

26 Guo, R., Jho, Y.-D. & Minnich, A. J. Coherent control of thermal phonon transport in van der Waals superlattices. *Nanoscale* **10**, 14432-14440 (2018). https://doi.org:10.1039/C8NR02150C

27 Solanki, G. K., Gujarathi, D. N., Deshpande, M. P., Lakshminarayana, D. & Agarwal, M. K. Transport Property Measurements in Tungsten Sulphoselenide Single Crystals Grown by a CVT Technique. *Cryst. Res. Technol.* **43**, 179-185 (2008). https://doi.org:https://doi.org/10.1002/crat.200711060

28 Lee, C., Hong, J., Whangbo, M.-H. & Shim, J. H. Enhancing the Thermoelectric Properties of Layered Transition-Metal Dichalcogenides 2H-MQ_2 (M = Mo, W; Q = S, Se, Te) by Layer Mixing: Density Functional Investigation. *Chem. Mater.* **25**, 3745-3752 (2013). https://doi.org:10.1021/cm402281n

29 Jiang, P., Qian, X., Gu, X. & Yang, R. Probing Anisotropic Thermal Conductivity of Transition Metal Dichalcogenides MX_2 (M = Mo, W and X =

S, Se) using Time-Domain Thermoreflectance. *Adv. Mater.* **29**, 1701068 (2017). https://doi.org:https://doi.org/10.1002/adma.201701068

30 Lindroth, D. O. & Erhart, P. Thermal Transport in Van der Waals Solids from First-principles Calculations. *Phys. Rev. B* **94**, 115205 (2016).

31 Liu, L., Kumar, S. B., Ouyang, Y. & Guo, J. Performance Limits of Monolayer Transition Metal Dichalcogenide Transistors. *IEEE T. Electron Dev.* **58**, 3042-3047 (2011). https://doi.org:10.1109/TED.2011.2159221

32 Peng, B. *et al.* Thermal conductivity of monolayer MoS 2, MoSe 2, and WS 2: interplay of mass effect, interatomic bonding and anharmonicity. *RSC adv.* **6**, 5767-5773 (2016).

33 Chen, J., Walther, J. H. & Koumoutsakos, P. Strain Engineering of Kapitza Resistance in Few-Layer Graphene. *Nano Lett.* **14**, 819-825 (2014). https://doi.org:10.1021/nl404182k

34 Plimpton, S. Fast Parallel Algorithms for Short-Range Molecular Dynamics. *J. Comput. Phys.* **117**, 1-19 (1995). https://doi.org:https://doi.org/10.1006/jcph.1995.1039

35 Ueno, T., Rhone, T. D., Hou, Z., Mizoguchi, T. & Tsuda, K. COMBO: An Efficient Bayesian Optimization Library For Materials Science. *Mater. Discovery* **4**, 18-21 (2016). https://doi.org:https://doi.org/10.1016/j.md.2016.04.001

36 Ong, Z.-Y. Atomistic S-matrix Method for Numerical Simulation of Phonon Reflection, Transmission, and Boundary Scattering. *Phys. Rev. B* **98**, 195301 (2018). https://doi.org:10.1103/PhysRevB.98.195301

37 Baroni, S., de Gironcoli, S., Dal Corso, A. & Giannozzi, P. Phonons and Related Crystal Properties From Density-functional Perturbation Theory. *Rev. Mod. Phys.* **73**, 515-562 (2001). https://doi.org:10.1103/RevModPhys.73.515

38 Royo, M. & Rurali, R. Tuning thermal Transport in Si Nanowires by Isotope Engineering. *Phys. Chem. Chem. Phys.* **18**, 26262-26267 (2016). https://doi.org:10.1039/C6CP04581B

39 Zhang, W., Fisher, T. S. & Mingo, N. The Atomistic Green's Function Method: An Efficient Simulation Approach for Nanoscale Phonon Transport. *Numer. Heat Tr. B-Fund.* **51**, 333-349 (2007). https://doi.org:10.1080/10407790601144755

40 Zhang, W., Fisher, T. S. & Mingo, N. Simulation of Interfacial Phonon Transport in Si–Ge Heterostructures Using an Atomistic Green's Function Method. *J. Heat Transfer.* **129**, 483-491 (2006). https://doi.org:10.1115/1.2709656

41 Yang, L., Latour, B. & Minnich, A. J. Phonon Transmission at Crystalline-amorphous Interfaces Studied Using Mode-resolved Atomistic Green's Functions. *Phys. Rev. B* **97**, 205306 (2018). https://doi.org:10.1103/PhysRevB.97.205306

42 Dhar, A. & Roy, D. Heat Transport in Harmonic Lattices. *J. Stat. Phys.* **125**, 801-820 (2006). https://doi.org:10.1007/s10955-006-9235-3

43 Zhu, G. *et al.* Tuning thermal conductivity in molybdenum disulfide by electrochemical intercalation. *Nature Communications* **7**, 13211 (2016). https://doi.org:10.1038/ncomms13211

44 Sadeghi, M. M., Jo, I. & Shi, L. Phonon-interface Scattering in Multilayer Graphene on an Amorphous Support. *P. NatL. A. Sci.* **110**, 16321-16326 (2013). https://doi.org:10.1073/pnas.1306175110

45 Seol, J. H. *et al.* Two-Dimensional Phonon Transport in Supported Graphene. *Science* **328**, 213-216 (2010). https://doi.org:10.1126/science.1184014

46 Wang, Z. *et al.* Thermal Transport in Suspended and Supported Few-Layer Graphene. *Nano Lett.* **11**, 113-118 (2011). https://doi.org:10.1021/nl102923q

47 Ong, Z.-Y., Zhang, G. & Zhang, Y.-W. The Role of Flexural Coupling in Heat Dissipation from a Two-dimensional Layered Material to its Hexagonal Boron Nitride Substrate. *2D Mater.* **8**, 035032 (2021). https://doi.org:10.1088/2053-1583/abf98f

48 Lindsay, L., Broido, D. A. & Mingo, N. Flexural Phonons and Thermal Transport in Multilayer Graphene and Graphite. *Phys. Rev. B* **83**, 235428 (2011). https://doi.org:10.1103/PhysRevB.83.235428

49 Taheri, A., Pisana, S. & Singh, C. V. Importance of quadratic dispersion in acoustic flexural phonons for thermal transport of two-dimensional materials. *Phys. Rev. B* **103**, 235426 (2021). https://doi.org:10.1103/PhysRevB.103.235426

50 Gospodarev, I. A., Kravchenko, K. V., Syrkin, E. S. & Feodos'ev, S. B. Quasi-two-dimensional features in the phonon spectrum of graphite. *Low Temp. Phys.* **35**, 589-595 (2009). https://doi.org:10.1063/1.3170936

51 Feodosyev, S. B. *et al.* Propagation and localization of phonons in graphite and graphene nanofilms. *Low Temp. Phys.* **48**, 121-125 (2022). https://doi.org:10.1063/10.0009291

52 Hazrati, E., de Wijs, G. A. & Brocks, G. Li intercalation in graphite: A van der Waals density-functional study. *Phys. Rev. B* **90**, 155448 (2014). https://doi.org:10.1103/PhysRevB.90.155448

53 Karssemeijer, L. J. & Fasolino, A. Phonons of graphene and graphitic materials derived from the empirical potential LCBOPII. *Surf. Sci.* **605**, 1611-1615 (2011). https://doi.org:https://doi.org/10.1016/j.susc.2010.10.036

54 Wirtz, L. & Rubio, A. The phonon dispersion of graphite revisited. *Solid State Commun.* **131**, 141-152 (2004). https://doi.org:https://doi.org/10.1016/j.ssc.2004.04.042

55 Gan, C. K. & Ong, Z.-Y. Complementary local-global approach for phonon mode connectivities. *J. Phys. Commun.* **5**, 015010 (2021). https://doi.org:10.1088/2399-6528/abd8ed

56 Chen, G. Phonon Wave Heat Conduction in Thin Films and Superlattices. *J. Heat Transfer.* **121**, 945-953 (1999). https://doi.org:10.1115/1.2826085

57 Chen, G. *Nanoscale Energy Transport and Conversion: a Parallel Treatment of Electrons, Molecules, Phonons, and Photons*. (Oxford university press, 2005).

58 Altfeder, I., Voevodin, A. A. & Roy, A. K. Vacuum Phonon Tunneling. *Phys. Rev. Lett.* **105**, 166101 (2010). https://doi.org:10.1103/PhysRevLett.105.166101

59 Chiloyan, V., Garg, J., Esfarjani, K. & Chen, G. Transition From Near-field Thermal Radiation to Phonon Heat Conduction at Sub-nanometre Gaps. *Nat. Commun.* **6**, 6755 (2015). https://doi.org:10.1038/ncomms7755